A 2-V 600-μA 1-GHz BiCMOS Super-Regenerative Receiver for ISM Applications

Patrick Favre, *Member, IEEE*, Norbert Joehl, Alexandre Vouilloz, Philippe Deval, Catherine Dehollain, *Member, IEEE*, and Michel J. Declercq, *Senior Member, IEEE*

***Abstract*—A 1-GHz receiver, integrated in a 0.8-μm BiCMOS technology, consumes 1.2 mW at 2 V. Based on super-regeneration, it is dedicated to short-range data exchange up to 100 kbits/s. Sensitivity of -98 dBm is achieved for a selectivity of 100 kHz. The size of the chip is smaller than 1 mm^2.**

I. Introduction

THE high-volume demand for wireless short-distance data-exchange components for applications such as home automation, robotics, computer peripherals, or biomedicine requires an electronic board with a small number of electronic components and an optimized cost for the receiver chip. The reduction of the number of components is not only needed in terms of cost but also in terms of reliability. The cost and size reduction in a receiver implies a design without all the big and expensive components like ceramic or surface acoustic wave (SAW) filters.

The presented circuit responds to this demand by making use of an original architecture based on the super-regeneration principle which was invented by Armstrong in 1922 [1]. This technique was widely used in vacuum tube circuits until the 1950's. Then it was progressively abandoned for the superheterodyne receiver due to its better selectivity. Nowadays, original analog integrated circuit techniques make possible a great improvement of the bandwidth and of the sensitivity of modern super-regenerative receivers.

Low-range data transmissions generally make use of the UHF industrial, scientific, and medical (ISM) bands, centered at 916 MHz in the United States and at 433.92 MHz in Europe. Those bands are characterized by a strong overcrowding, and for this reason a half-duplex link is generally needed. In this case the receiver will be battery operated, resulting in an operating voltage range extending from 2 V to 3.2 V in the case of a two-cell operation. A small current consumption of the receiver is essential in order to extend the life of the operated device.

Typical data rates for ISM applications are usually smaller than 20 kbit/s; however, a higher bandwidth in the receiver can reduce the current consumption. Currently, a good power management associated with a small duty cycle between operation mode and sleep mode can reduce effectively the average current consumption. For this reason, a bandwidth as wide as 100 kHz can be useful for this kind of application.

Manuscript received May 7, 1998; revised July 20, 1998.

The authors are with EPFL-LEG-ELB ECUBLENS, Lausanne CH-1015 Switzerland.

Publisher Item Identifier S 0018-9200(98)08605-3.

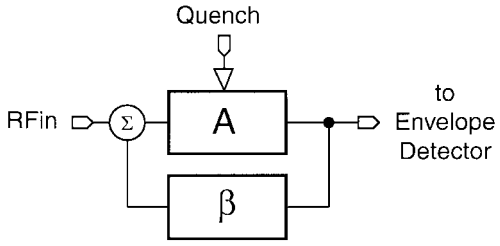

Fig. 1. Block schematic.

The small size of the device means that a small antenna with a poor efficiency will be used. To achieve good performance in those conditions, a high sensitivity is necessary, which conflicts with the circuit design requirements for low consumption. For this reason, a tradeoff has to be found in order to satisfy the two requirements. In this tradeoff we have to consider that the typical transmission range is smaller than 20 m, and the typical radiated power is smaller than 100 μW in order to comply with Federal Communication Commission (FCC) and European Telecommunication Standards Institute (ETSI) regulations.

The low-cost option implies a reduction in the silicon size. A really consequential reduction can only be achieved through the suppression of double paths like in in-phase quadrature (IQ) systems. Size consuming filters like the bandpass or lowpass present in zero intermediate frequency (IF) or low IF should also be avoided.

Current solutions, generally based on conversion systems, like zero-IF or low-IF receivers, are penalized by their power consumption, their minimum operating voltage, and the number of external components. In this work, the receiver is based on the super-regeneration principle. Due to the simplified architecture of the circuit, a 2-V 1.2-mW chip has been integrated on a 6-GHz 0.8-μm BiCMOS technology. The external components are limited to the resonator and to decoupling capacitors.

II. Super-Regenerative Receiver Principles

A. Block Schematic

Fig. 1 shows the principle of a super-regenerative receiver. The system is an oscillator, constituted by the gain block A and by the selective feedback network β. Two external signals are connected to this oscillator.

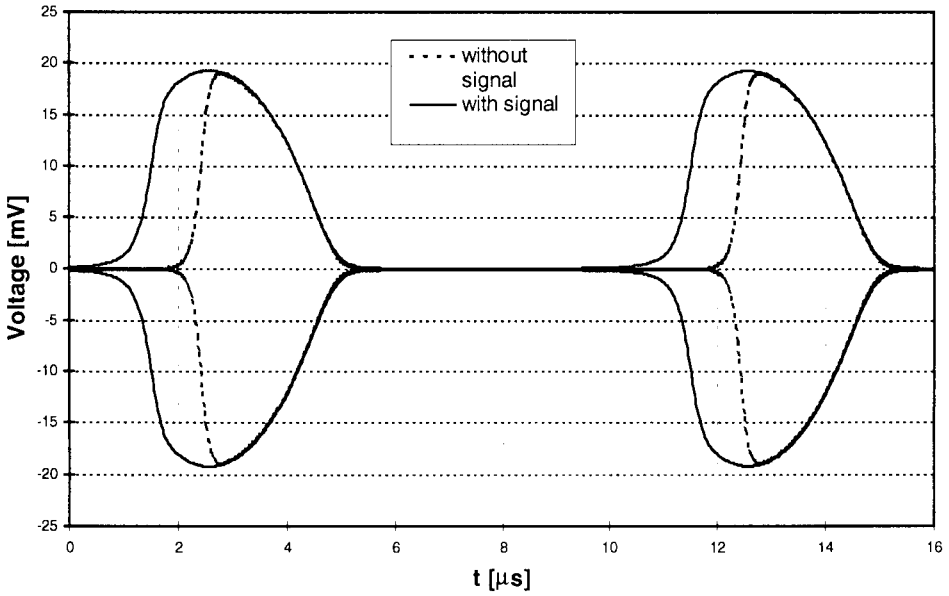

Fig. 2. Envelope of the oscillator.

The RF input is the terminal connected to the antenna. It will introduce energy coming from the antenna to the oscillator, modifying its start-up behavior.

The quench signal is a control signal generated internally. Its purpose is to modify periodically the close-loop gain of the system, removing or restoring sequentially the oscillation conditions.

Without RF signals introduced in the system, the start-up time of the oscillator is fixed by the different parameters of the system. They are the unloaded quality factor Q of the feedback network, the gain of the amplifier (controlled by the quench signal), and the amount of thermal noise present in the circuit. A signal injected in the oscillator will modify the start-up time, the level of the modification will depend on the gap between its frequency and the frequency of the oscillator and on its power level. The measurement of the start-up time of this oscillator is an image of the amount of RF signal injected close to the natural frequency of the oscillator.

Fig. 2 shows the difference in the start-up time with and without an input signal. The start-up time varies with the input level. Due to the difficulty of measuring accurately the start-up time of an oscillator, the oscillator is turned on and off periodically, and this measurement is replaced by the detection of the mean value of the oscillator.

B. Main Signals Diagram

Fig. 3 shows the main signals of the circuit. The first line shows the RF input signal, which is 100% amplitude modulated by the data. Generally, it is on–off keying (OOK) modulated.

The second line presents the quench signal, the period of which is smaller than the period of the data. This system behaves like a sampled system in that the data are sampled by the quench signal.

The third line presents the shape of the oscillations at the output of the oscillator. Start-up delay of the oscillator changes with the amount of RF input signal.

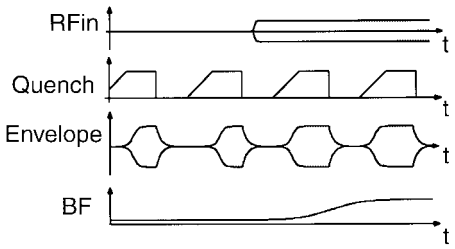

Fig. 3. Main signals diagram.

The last line presents the demodulated output, which is obtained by lowpass filtering the detected output signal of the oscillator.

C. Modes of Operation

Super-regenerative receivers have two possible modes of operation. The logarithmic mode is characterized by a logarithmic relation between the amplitude of the RF input signal and the amplitude of the demodulated output. In this mode, the oscillator reaches its steady-state amplitude at each quench cycle due to a low quench frequency and/or a high start-up current. This mode is characterized by a reduced dynamic range of the demodulated output due to the logarithmic compression of the signal.

Linear mode is characterized by a linear relation between the amplitude of the RF input signal and the amplitude of the demodulated output. In this mode, the oscillator does not reach its steady-state during the quench period, due to a high quench frequency and/or a low start-up current.

Typical operation is usually made of a mixture of those modes. This implies that it is difficult to find an exact mathematical model. The transition from one mode to another is due to a change in a parameter of the quench signal, like amplitude, frequency, duty-cycle, or mean level.

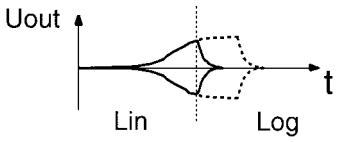

Fig. 4. Envelope of the oscillator.

Fig. 4 shows the envelope of the output of the oscillator for the linear mode and the logarithmic mode.

Note that besides the super-regenerative mode of operation, the same circuit could also work in the "regenerative" mode. In this mode, the bias current of the receiver is smaller than the current needed to cancel all the losses. The result is a Q-enhanced selective amplifier. The value of the bias current of the oscillator fixes the quality factor Q of the amplifier. The detection gain of the regenerative mode is more than 10 times higher than the super-regenerative gain. The limitation of this mode of operation resides in the difficulty to control its Q factor. The presented circuit has been used in a pseudoregenerative mode, which is a mixture between the super-regenerative and the regenerative mode, exhibiting Q values up to 10 000.

FM discrimination can be achieved by centering the edge of the selectivity curve at the desired frequency. However, this method suffers from many drawbacks: the maximum sensitivity frequency is not the desired frequency and the demodulation gain is very weak due to the slope of the selectivity curve of the super-regenerative receiver. The drawbacks of the FM discrimination explain why it has been decided to use a 100% AM (OOK) modulation.

III. Theory of Super-Regeneration

The principle of super-regeneration is summarized in Fig. 5. A negative conductance $-g_m/2$ is varied periodically in parallel with a resonant circuit. The losses of the *LC* resonator are simulated by a positive conductance g_{LC}. This simple model is only valid for frequencies near the resonant frequency f_0. The equivalent conductance $g(t)$, in parallel with the inductance and the capacitor, is equal to the sum of the negative (active) and positive (passive) conductances

$$g(t) = g_{\mathrm{LC}} - \frac{g_m(I)}{2} \tag{1}$$

$$\overline{g(t)} = f_g \cdot \int_{f_0}^{f_0+1/r_4} g(t)\cdot dt \quad \overline{g(t)} > 0 \text{ for stability.} \tag{2}$$

It must be noticed that the following theory is only valid in linear mode. The transient behavior of the circuit can therefore be described by

$$\frac{d^2\Delta v}{dt^2} + 2\cdot\frac{d\Delta v}{dt}\cdot\underbrace{\frac{g(t)}{2\cdot C}}_{\omega(t)} + \left(\omega_0^2 + 2\cdot\frac{d\omega(t)}{dt}\right)\cdot\Delta v = -\frac{1}{C}\cdot\frac{di_s}{dt}$$

with

$$\omega_0 = \frac{1}{\sqrt{2\cdot L\cdot C}}. \tag{3}$$

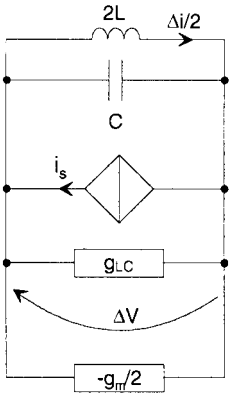

$$g(t) = g_{LC} - \frac{g_m(t)}{2} \quad (1)$$

$$\overline{g(t)} = f_q \cdot \int_{t_0}^{t_0+1/f_q} g(t)\cdot dt \quad (2)$$

$$\overline{g(t)} > 0 \text{ for stability}$$

Fig. 5. Super-regeneration principle.

The current source i_s represents the RF input signal. It is given by $i_s = I_s\sin(\omega_s t)$.

If g is supposed positive and constant, the differential equation (3), which describes mathematically the behavior of the circuit, has a stable solution. This means that the free oscillation is damped with a time constant equal to $\tau = 1/\omega = 2\cdot C/g$ and the circuit works like a filter (forced oscillation is dominant). When g is negative, it behaves like an oscillator (free oscillation is dominant) with the growing time constant equal in absolute value to the one of the filter.

In a super-regenerative receiver, g varies periodically below and above zero at a frequency f_q. The mean value $\overline{g(t)}$ must be greater than zero for stable operation. Equation (3) is a typical case of a time-varying differential equation, which provides a solution in the form of [2]–[4]

$$\Delta v = \Delta u\cdot e^{-\int_0^t \omega(t)\,dt} \rightarrow \frac{d^2\Delta u}{dt^2} + \Delta u\cdot\left(\omega_0^2 - \omega^2(t) + \frac{d\omega(t)}{dt}\right) = \underbrace{-\frac{1}{C}\cdot\frac{di_s}{dt}\cdot e^{\int_0^t \omega(t)\,dt}}_{\psi(t)}. \tag{4}$$

Thus

$$\Delta v = e^{-\int_0^t \omega(t)\,dt}\cdot\left[\alpha\cdot\cos(\omega_0\cdot t) + \beta\cdot\sin(\omega_0\cdot t) + \frac{1}{\omega_0}\cdot\int_0^t \psi(x)\cdot\sin[\omega_0\cdot(t-x)]\cdot dx\right] \quad \text{if } \omega_0^2 \gg |\dot{\omega} - \omega^2|. \tag{5}$$

This expression is too general to be solved analytically. The resolution must be divided into two cases: the *slope* and *step* controlled modes. The first one makes the assumption that the variation of the conductance $\dot{g}(t_k)$ is slow when $g(t_k) = 0$ $(k = 1,2,3,\cdots)$, and in the second one, it is supposed that this variation is very steep. Two particular solutions to this problem have been found by Macfarlane and Whitehead [3].

It is interesting to find the solution for typical quench signal like the sawtooth, triangular, sinusoidal and square wave forms. To reduce and to normalize the equation, it is necessary

TABLE I

	Sinusoidal wave quench	Square wave quench
	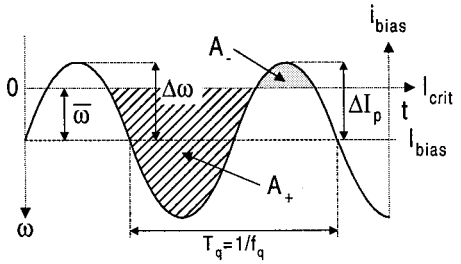	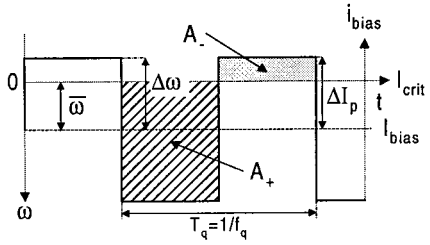
Magnitude frequency response	$S(\Delta\Omega_s)=\left(1+\Delta\Omega_s\cdot\frac{\bar{\omega}}{\omega_0}\right)\cdot e^{-\frac{(\bar{\omega}\cdot\Delta\Omega_s)^2}{2\cdot\bar{\omega}(t_x)}}\cong\exp\left(-\frac{\Omega_s^2}{2\cdot\Omega_q\cdot\sqrt{\Delta\Omega^2-1}}\right)$	$S(\Delta\Omega_s)\cong\frac{\Delta\Omega^2-1}{\sqrt{\left[\Omega_s{}^2+(\Delta\Omega+1)^2\right]\cdot\left[\Omega_s{}^2+(\Delta\Omega-1)^2\right]}}$
Bandwidth	$BW_{-20\cdot\log_{10}(\mu)}=\sqrt{8\cdot\ln\mu}\cdot f_q\cdot\frac{\sqrt[4]{\Delta\Omega^2-1}}{\sqrt{\Omega_q}}$	$BW_{-20\cdot\log_{10}(\mu)}=\frac{2}{\Omega_q}\cdot\left[\mu\cdot\sqrt{\left(\Delta\Omega^2-1\right)^2+\frac{4\cdot\Delta\Omega^2}{\mu^2}}-\Delta\Omega^2-1\right]^{1/2}$
Bandwidth at - 3dB	$BW_{-3dB}=1.6651\cdot f_q\cdot\frac{\sqrt[4]{\Delta\Omega^2-1}}{\sqrt{\Omega_q}}$	$BW_{-3dB}=\frac{2}{\Omega_q}\cdot\left[\sqrt{2\cdot\left(\Delta\Omega^4+1\right)}-\Delta\Omega^2-1\right]^{1/2}$
Superregenerative gain G_s	$G_s\cong\frac{e^{A_-}}{\sqrt{\Delta\Omega^2-1}}$	$G_s\cong\frac{\Delta\Omega^{0.4}}{\Delta\Omega-1}\cdot\left[\frac{1}{\pi}\cdot\frac{\Delta\Omega\cdot\Omega_q}{\Delta\Omega^2-1}\cdot\left(e^{A_-}-1\right)-\frac{1}{2}\right]$
Surface A	$A_-=\frac{2\cdot\sqrt{\Delta\Omega^2-1}+2\cdot\arcsin(1/\Delta\Omega)-\pi}{\Omega_q}$	$A_-=\pi\cdot\frac{\Delta\Omega-1}{\Omega_q}$

to introduce the following notation:

$$\Omega_q=\frac{\omega_q}{\bar{\omega}}=2\cdot Q_r\cdot\frac{\omega_q}{\omega_0}$$

and

$$\Delta\Omega=\frac{\Delta\omega}{\bar{\omega}}=\frac{\Delta g}{\bar{g}}=Q_r\cdot\frac{\Delta g}{C\cdot\omega_0}$$

- f_0 resonant frequency = central frequency of reception;
- f_g RF input signal frequency;
- Δf_g $f_g - f_0$ = gap between the RF input and the resonant frequencies;
- ω_q $2\cdot\pi\cdot f_q$ with f_q = quench wave frequency;
- $Q_{\rm LC}$ $\frac{C\cdot\omega_0}{g_{\rm LC}}$ = quality factor of the resonant circuit;
- Q_r $\frac{C\cdot\omega_0}{\bar{g}}=\frac{\omega_0}{2\cdot\bar{\omega}}$ = quality factor due to the regenerative effect;
- $\bar{\omega}$ $\frac{\bar{g}}{2\cdot C}=\frac{1}{\bar{\tau}}$ = mean damping frequency (see Tables I and II);
- $\Delta\omega$ $\frac{\Delta g}{2\cdot C}=\frac{1}{\Delta\tau}$ = difference between the mean and the minimum damping frequency factor (see Tables I and II);
- A_- area under the negative portion of the damping frequency time curve;
- A_+ area above the positive portion of the damping frequency time curve.

With these notations, it is possible to calculate the bandwidth (BW) in Hz and the super-regenerative gain $G_s = \bar{U}/(I_s/\bar{g})$ between the voltage output of the filter $\bar{U}$ and the input RF voltage. The results are summarized in Table I.

With the circuit of Fig. 6, the main variables become

$$\Omega_q=\frac{8\cdot C\cdot\omega_q\cdot U_T}{I_{\rm crit}-I_{\rm bias}}\cdot\frac{\beta+1}{\beta-1},\quad \Delta\Omega=\frac{\Delta I_p}{I_{\rm crit}-I_{\rm bias}}$$
$$\bar{\omega}=\frac{I_{\rm crit}-I_{\rm bias}}{8\cdot C\cdot U_T}\cdot\frac{\beta-1}{\beta+1},\quad \Delta\omega=\frac{\Delta I_p}{8\cdot C\cdot U_\tau}\cdot\frac{\beta-1}{\beta+1}$$
$$Q_r=\frac{4\cdot C\cdot\omega_0\cdot U_\tau}{I_{\rm crit}-I_{\rm bias}}\cdot\frac{\beta+1}{\beta-1}$$
$$I_{\rm crit}=\frac{4\cdot C\cdot\omega_0\cdot U_\gamma}{Q_{\rm LC}}\cdot\frac{\beta+1}{\beta-1},\quad G_r=\frac{I_{\rm crit}}{I_{\rm crit}-I_{\rm bias}}.$$

It must be noticed that all the equations given in Tables I and II are obtained with the assumption that the free oscillation contribution to the gain is greater than the forced one. It implies that the ratio $\Delta\Omega$ between the quench current amplitude and the critical current minus the bias current is about greater than one. The quench frequency must also not be too high to let time to the free oscillation to start (Ω_q ratio limited).

This analysis shows the importance of the quench signal. The selectivity and the sensitivity are directly controlled by the quench parameters. The critical parameters of the quench signal are its shape, its frequency, its amplitude, and its mean value. The most important parameter is the slope of the quench current during the crossing of the critical current value, this slope has to be small in order to improve the selectivity.

Selectivity is related to the quench frequency with a relation of the form of $1/\sqrt{\omega_q}$ (except in the case of the square wave

TABLE II

	Triangular wave quench	Saw-tooth wave quench
	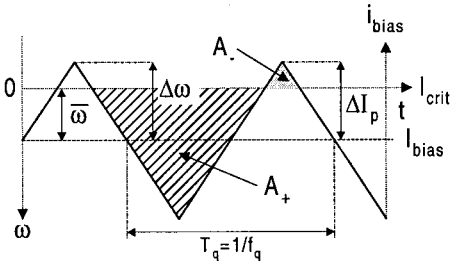	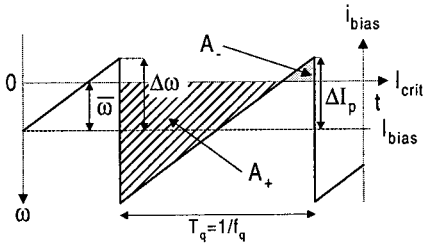
Magnitude frequency response	$S(\Delta\Omega_s) \cong \exp\left(-\frac{\pi}{4}\cdot\frac{\Omega_s^2}{\Omega_q\cdot\Delta\Omega}\right)$	$S(\Delta\Omega_s) \cong \exp\left(-\frac{\pi}{2}\cdot\frac{\Omega_s^2}{\Omega_q\cdot\Delta\Omega}\right)$
Bandwidth	$BW_{-20\cdot\log_{10}(\mu)} = 4\cdot\sqrt{\frac{\ln\mu}{\pi}}\cdot f_q\cdot\sqrt{\frac{\Delta\Omega}{\Omega_q}}$	$BW_{-20\cdot\log_{10}(\mu)} = \sqrt{\frac{8\cdot\ln\mu}{\pi}}\cdot f_q\cdot\sqrt{\frac{\Delta\Omega}{\Omega_q}}$
Bandwidth at - 3dB	$BW_{-3dB} = 1.3286\cdot f_q\cdot\sqrt{\frac{\Delta\Omega}{\Omega_q}}$	$BW_{-3dB} = 0.9394\cdot f_q\cdot\sqrt{\frac{\Delta\Omega}{\Omega_q}}$
Superregenerative gain G_s	$G_s \cong \frac{\pi}{2}\cdot\frac{e^{A_-}}{\Delta\Omega}$	$G_s \cong \frac{\sqrt{2\cdot\Omega_q\cdot\Delta\Omega}}{\Delta\Omega^2-1}\cdot e^{A_-}$
Surface A	$A_- = \frac{\pi}{2}\cdot\frac{(\Delta\Omega-1)^2}{\Omega_q\cdot\Delta\Omega}$	$A_- = \frac{\pi}{2}\cdot\frac{(\Delta\Omega-1)^2}{\Omega_q\cdot\Delta\Omega}$

quench for which the selectivity is independent of ω_q). For this reason, the quench frequency has to be minimized. However, due to the Nyquist criterion, this frequency has to be at least twice the maximum data frequency. The relation between the selectivity and the quench peak value ΔI_p has the form of $\sqrt{\Delta I_p}$ (except in the case of the square-wave quench: see Tables I and II for more details).

Sensitivity of the receiver is proportional to the gain of the circuit, called the "super-regenerative gain." This gain is defined as the ratio between the average voltage at the output of the envelope detector and the RF input voltage injected in the parallel resonant circuit. It is proportional to the area of the quench current above the critical point (A-). Thus the gain is greater for the square wave quench than for the slope-type quench. A compromise has to be found between the selectivity and the sensitivity: a high sensitivity implies a high A- area, while a high selectivity needs a low A- area.

The main problem with super-regenerative receivers is their selectivity limitation due to the sampled mode of operation. In a classical superheterodyne receiver, it is possible to demodulate two adjacent signals separated by a bandwidth twice the binary data-rate in OOK. In the case of the super-regenerative receiver, this is not possible because the minimum value of the quench frequency is equal to two times the data frequency (Nyquist criterion), more in practice, and it is not possible to decrease the bandwidth below two times the quench frequency. Thus, in practice, the bandwidth will be 20 times the binary data rate.

The only way to overcome this limitation is to make use of regeneration instead of super-regeneration. The major problem of this mode is the tight control of the Q of the receiver. The Q being fixed by the gap between the critical current and the bias current of the "regenerator."

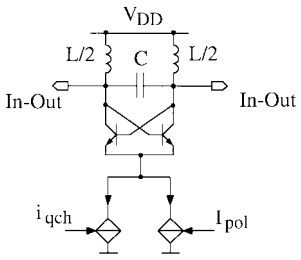

Fig. 6. Oscillator schematic.

IV. Design and Optimization of the Receiver

A. Oscillator

The oscillator of the super-regenerative receiver is based on the schematic of Fig. 6. The differential pair, with cross-coupled bases, generates a negative resistance connected to an LC resonator. The value of the real part of the impedance presented to the resonator is given by

$$\mathrm{Re}(Z_{\mathrm{in}}) = \frac{-2}{g_m}$$

g_m being the transconductance of each bipolar transistors of Fig. 6.

This structure has the following two modes of operation:

$$\text{oscillator if } \frac{g_m}{2} \geq g_0$$

$$\text{filter if } \frac{g_m}{2} < g_0.$$

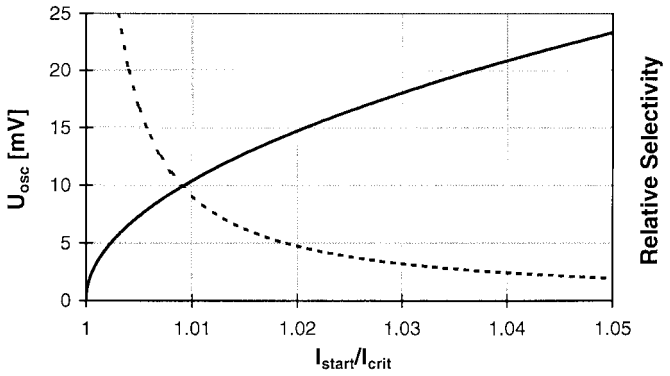

Fig. 7. Relation between current and amplitude in the oscillator.

Its current consumption is inversely proportional to the unloaded Q of the resonator. The differential structure of the oscillator ensures a high common mode rejection ratio. The bias current of the oscillator is provided by two sources. The first one, $I_{\rm pol}$, gives the DC operating point and the second one, $i_{\rm qch}$, represents the AC quench current.

The differential pair of bipolar transistors is a nonlinear element. Amplitude limitation depends on those nonlinearities. The distortion increases with amplitude, thereby reducing the g_m. Amplitude stabilization occurs when $g_m/2 = g_0$. The critical current of such an oscillator is defined as the current for which $g_m/2 = g_0$ for an output amplitude equal to zero.

B. Operating Point Control

The optimization of the selectivity of the receiver is based on the control of the operating current of the oscillator. The gap between its start-up current and its critical current has to be minimized. The position of this operating point can be controlled through the measurement of the output level of the oscillator. The solid line in Fig. 7 shows the relation between this gap and the saturation amplitude of the oscillator. The chip presented in this paper will use an amplitude locked loop to control the operating point.

The dashed line of Fig. 7 shows the variation of the selectivity of the receiver as a function of the ratio between the critical and the peak quench current. High selectivities are obtained for small gaps and thus for small output amplitude of the oscillator. One limit of super-regenerative receivers is shown here: very high selectivity implies undetectable output level of the oscillator. The presented design makes use of a $\Delta I_{\rm start}/I_{\rm crit}$ of 1%, with an amplitude of 10 mV. The parameter $\Delta I_{\rm start}$ is equal to $(I_{\rm start} - I_{\rm crit})$.

C. Capacitive Voltage Boosting

Amplitude detection of a 10 mV signal at 1 GHz is unrealistic without amplification. Amplifiers realized in this 0.8 μm BiCMOS technology exhibit a gain-bandwidth product smaller than 1 GHz. The accuracy of the voltage gain of the amplifier is then insufficient for a tight control of the operating point. However, it is possible to overcome this problem by extending the dynamic range of the oscillator.

To simplify the analysis of the oscillator, the base current and the collector-base capacitance will be neglected. The schematic diagram of Fig. 8 shows the principle of the voltage boosting. The output amplitude, for a given gap between the critical and the start-up current, will be increased by A_v. In this case, the "voltage gain" A_v of the structure is given by a capacitor ratio and is well controlled. It is expressed by

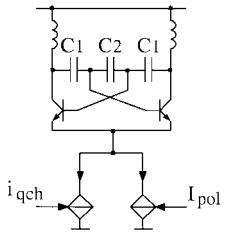

Fig. 8. Linearized oscillator.

$$A_v = 1 + \frac{2C_2}{C_1} \tag{6}$$

with

$$C_2 = nC_1.$$

The current consumption of this structure is boosted by a factor $1+2n$. The real part of the impedance presented by the differential pair to the inductors, is given by the following:

$$\mathrm{Re}(Z_{\rm in}) = -\frac{4n+2}{g_m}. \tag{7}$$

The control of the center frequency of the receiver is achieved through the control of the frequency of the oscillator. There is a gap between the frequency of reception and the frequency of the saturated oscillator. For a small level of quench current, this gap is smaller than the selectivity of the receiver.

Frequency control can be achieved by using any kind of resonator. A dielectric coaxial resonator improves the current consumption by a factor ten and insures the temperature stability of the receiver.

Phase-locked loop (PLL) control of the receiver is the best solution for high level of integration and for multichannel use. The oscillator of the super-regenerative receiver represents the voltage-controlled oscillator (VCO) of the PLL. However this VCO will be periodically turned on and off by the quench signal. For this reason, a sampled PLL has to be used. This original circuit has been evaluated and is currently in integration.

D. Block Diagram

Fig. 9 shows the architecture of the receiver. The block at the top of the diagram is the receiver itself. It is based on an oscillator, an envelope detector, and a lowpass filter (LPF).

The operating point control circuitry is shown at the bottom right of the diagram. The level of the oscillator output is sampled periodically and compared to a reference voltage. The result of the comparison conditions the operation of a charge pump circuit, injecting or taking off charge from an integrator depending on the amplitude of the oscillation. The output of the integrator drives a current source which controls the bias current of the oscillator.

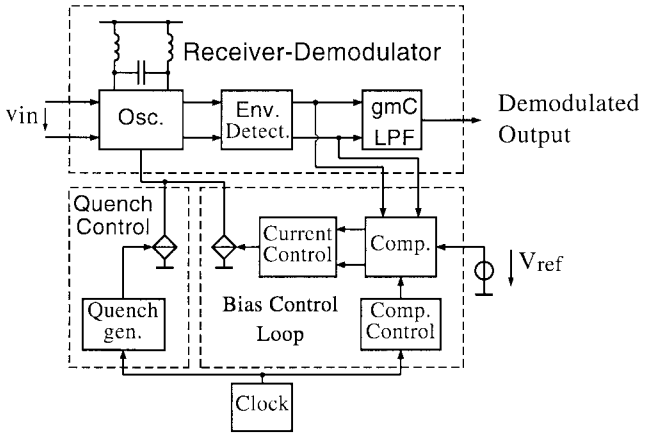

Fig. 9. Block diagram.

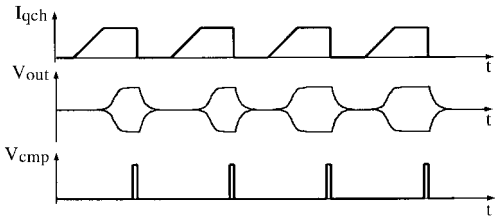

Fig. 10. Timing diagram.

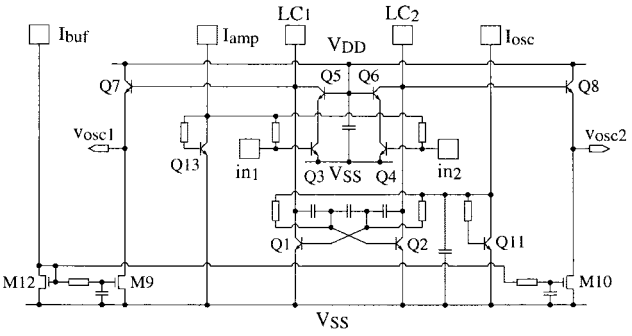

Fig. 11. Input amplifier and osillator.

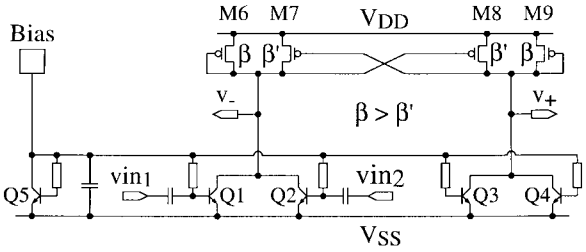

Fig. 12. Envelope detector.

The last block of the circuit diagram shows the quench control circuit. It is a simple sawtooth generator.

The timing diagram of Fig. 10 presents the principle signals used in the receiver. $I_{\rm qch}$ is the quench current, $V_{\rm out}$ the output of the oscillator, and $V_{\rm cmp}$ the clock applied to the sampling circuit. The pulses of $V_{\rm cmp}$ are placed at the end of the quench period in order to guarantee the saturation of the oscillator. The initial state of the bias current value has been fixed to 1 mA in order to guarantee a start-up time shorter than the quench period.

V. Detailed Schematics

A. Input Amplifier and Oscillator

The input amplifier and the oscillator use the same load (terminals $\rm LC_1$ and $\rm LC_2$) as shown in the schematic in Fig. 11. The input amplifier is based on a cascode structure to optimize its reverse isolation. It provides 39 dB of isolation between the oscillator and the antenna terminal at 1 GHz. Its input admittance has been simulated as

$$Y_{\rm in} = 36 + j160\ \mu\text{mhOs}.$$

The equivalent circuit for the input is a 1.7 kΩ resistor in parallel with a 30 fF capacitor at 916 MHz. The measured input impedance is $19 + j83\ \Omega$. This value is due to the impedance transformation by the printed circuit board and the package of the circuit. Qualification of the receiver has been achieved with an input matching network.

Noise figure and power gain concept cannot be used in this circuit because of the nonlinear load of the amplifier. This load can be represented by a RLC resonator, where R is the combination of the losses of the LC and the negative resistance provided by the differential cross-coupled pair (Q_1–Q_2). The value of this negative resistance is continuously modified by the quench signal.

The amplifier is biased by a 100-μA current to satisfy to a compromise between the sensitivity of the receiver and the low-power operation.

Low-voltage operation is improved by the base-biasing of the amplifier and the oscillator. Biasing is based on a current mirror between Q_1–Q_2–Q_{11} and Q_3–Q_4–Q_{13}. An emitter follower formed by Q_7–Q_8 and biased by M_9–M_{10} improves the isolation between the oscillator and the envelope detector.

Q_1 and Q_2 have a double-base structure for a noise-performance improvement. An emitter size of ten optimizes the current consumption. The optimal size of those transistors has been obtained by harmonic-balance simulations.

B. Envelope Detector

The schematic of the envelope detector is given in Fig. 12. The function of this circuit is to provide a voltage proportional to the rectified envelope of the input RF signal. Functionality is based on the exponential relation between the collector current and the base-emitter voltage of Q_1 and Q_2. This nonlinearity creates an increase of the mean collector current of Q_1 and Q_2 when an alternative voltage is applied on the base of Q_1 and Q_2. A differential structure presents a symmetrical load to the oscillator.

For a sinusoidal input signal, the mean value of the rise of the collector current $I_{Q1} + I_{Q2}$ is equal to

$$\Delta I = I_0 \cdot \sum_{n=1}^{\infty} \left[\frac{\left(\frac{U}{2 \cdot U_T}\right)^n}{2 \cdot n!} \right]^2$$

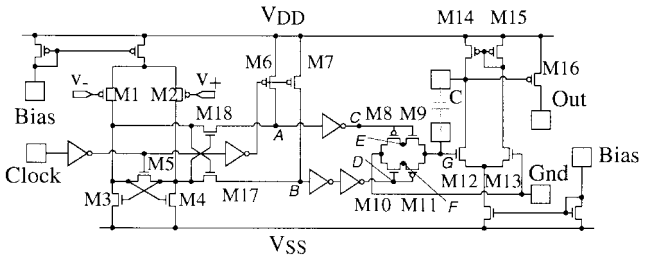

Fig. 13. Current-control circuit.

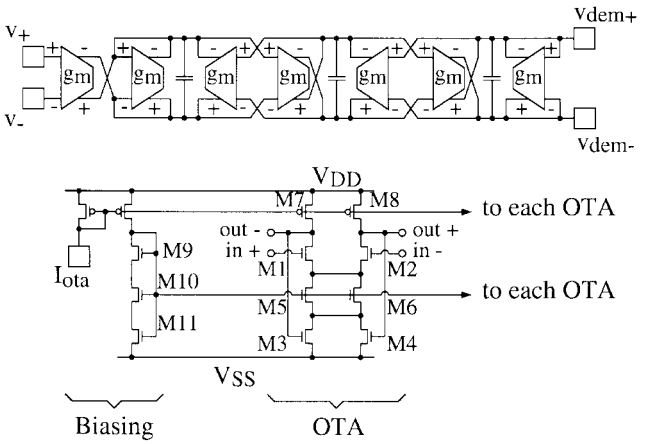

Fig. 14. G_m–C filter.

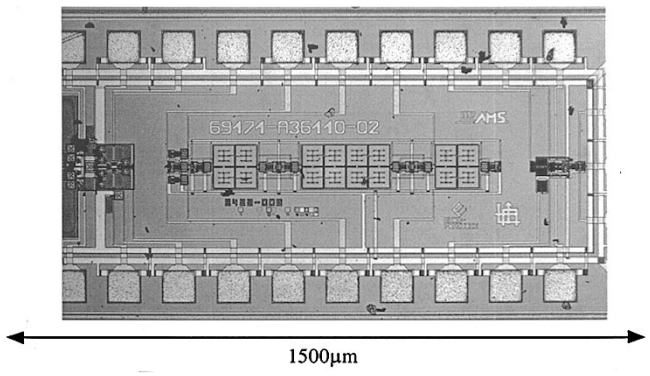

Fig. 15. Microphotography.

where I_0 is the DC bias current of Q_1 and Q_2 and U is the alternative voltage applied to the bases of Q_1 or Q_2.

The conversion of the current increase to a voltage increase is achieved by the cross-coupled structure Q_6 to Q_9 and the pair Q_3–Q_4. Q_3 and Q_4 are matched in size and current to Q_1 and Q_2.

The gain, or transresistance, of this structure is given by

$$\frac{\Delta V}{\Delta I} = \frac{1}{g_m} \cdot \frac{1+k}{1-k^2} \tag{8}$$

with

$$k = \frac{\beta'}{\beta}$$

and g_m being the transconductance of Q_6 and Q_9 and

$$\beta = \frac{W_{6,9}}{L_{6,9}} > \beta' = \frac{W_{7,8}}{L_{7,8}}.$$

If $\beta < \beta'$, the circuit is unstable.

Simulations and measurements show smaller detection gain than mathematically predicted. This is due to the high-frequency behavior of the transistor and the high voltage swing. This swing makes the effect of the channel length modulation non-negligible, and it can turn off Q_7 and put the gate of M_8 in conduction.

Simulation and measurement give a detection gain of this stage as high as ten for a bias current of 20 μA per transistor. The base-biasing of the structure improves the low voltage operation and the interstage isolation.

C. Current-Control Circuit

The current-control circuit is based on a charge-pump operation [6]. Its schematic is shown in Fig. 13. The goal of this circuit is to adjust the bias current of the oscillator. The adjustment is achieved when its steady-state amplitude reaches the desired value. This circuit is constituted by a sampled comparator and by a charge-pump circuit. The comparison time is determined by the clock signal. The result of the comparison conditions induces an injection (positive or negative) of charges in an integration capacitor. The voltage across this capacitor controls the bias current through M_{16}.

The charge pump operation is the following. It will be assumed that $V^+ > V^-$. When the clock signal changes from zero to one, M_5 is turned off and the drain of M_3 falls to V_{SS}. M_{17} is turned on and node B is therefore pulled down while node A remains close to V_{DD}. Node D changes from V_{DD} to V_{SS}. During the transition of node D, M_{10} is turned off first injecting a charge $-Q/2$ at node F. Then M_{11} is turned on, injecting a charge $-Q$ in the nodes F and G that are now short circuited. Q are the charges stored in the channel of the MOS transistor. At this point, a total amount of $-3Q/2$ is injected in the virtual ground G and integrated on the capacitor C. When the clock signal returns to zero, node D returns to V_{DD}. M_{11} turns off first, injecting a charge $+Q/2$ in nodes F and G, then M_{10} turns on discharging node F. Therefore the total amount of charges injected in node G at the end of the operation is equal to $-Q$. One can verify that when $V_+ < V_-$, a charge equal to $+Q$ is injected in node G after one clock pulse.

D. G_m–C LPF

The schematic diagram of the g_m–C LPF is given in Fig. 14 [7]. The filter has a third-order transfer function, based on a Butterworth polynomial. Its cutoff frequency is fixed by the bias current of the operational transconductance amplifiers. The transconductance amplifier is based on transistors M_1 and M_2. The circuit is biased by the current sources M_5 and M_6. The output common-mode voltage is stabilized by a regulation loop consisting of M_3 and M_4 which operate in conduction mode. Transistors M_7 and M_8 realize an active load.

M_1 and M_2 operate in weak inversion in order to improve their g_m/I ratio and thus the current consumption.

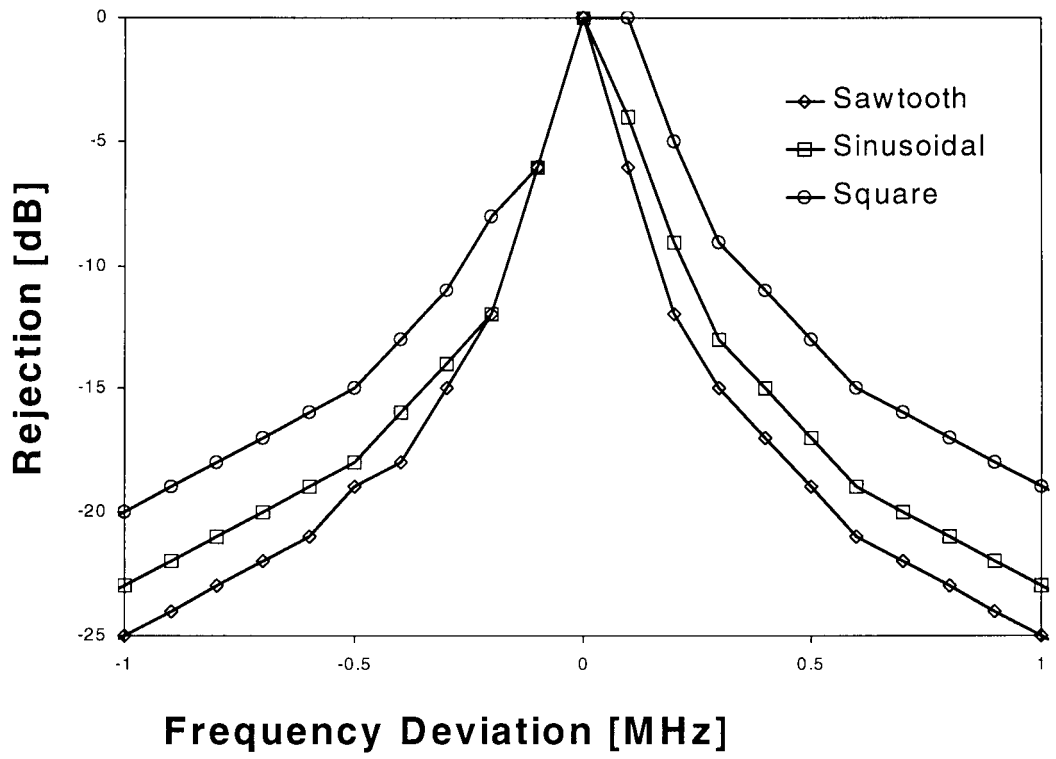

Fig. 16. Adjacent channel rejection as a function of the quench waveform, at 1 GHz center frequency.

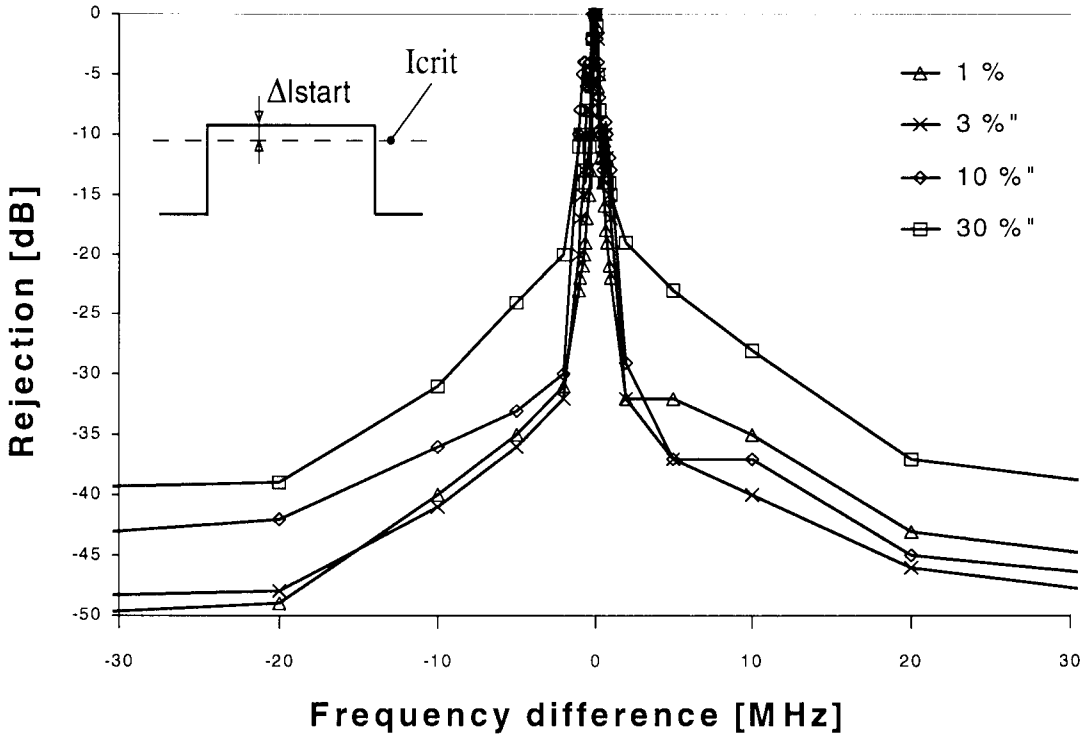

Fig. 17. Adjacent channel rejection as a function of the quench amplitude, at 1-GHz center frequency.

TABLE III
SUMMARY OF THE MEASUREMENTS

Min.Operating Voltage	2V
Supply Current	600 μA
Operating Frequency	300 to 1500MHz
Sensitivity	-98 dBm
Selectivity	100kHz
Input referred IP3	-25dBm
Silicon Size	< 1mm^2
Technology	0.8um, 6GHz f_t, BiCMOS

VI. LAYOUT

The layout microphotography is shown in Fig. 15. The super-regenerative receiver has been implemented in a 0.8-μm BiCMOS technology. The structure at the left of the circuit is the input amplifier and the oscillator, with its emitter followers. The tracks to the external resonator are 100 μm wide in order to optimize the Q of the resonator, and thus the current consumption. The central structure is the g_m–C LPF, and the circuit at the right of the layout is the bias-control circuitry. In this version, most of the pads are for test purposes. The size of the circuit has not been optimized. However, the total surface is smaller than 1 mm^2.

VII. MEASUREMENTS

A. Adjacent Channel Rejection Versus Quench Shape

Fig. 16 shows the curve of the adjacent channel rejection in relation with the quench waveform. This curve has been measured by applying a modulated RF signal to the receiver at a frequency different from the central frequency and by adjusting its level to get a 12 dB S/N ratio at the demodulated output.

This measurement shows that the selectivity is strongly dependent on the quench waveform. The best performances are achieved by the sawtooth quench, with a 100-kHz bandwidth at -3 dB.

B. Adjacent Channel Rejection Versus Quench Amplitude

Fig. 17 shows the adjacent channel rejection as a function of the relative gap between the critical and the start-up current ΔI_{start}.

The impact of the gap level appears strongly on this figure. The curve at 1% corresponds to the actual design parameter. Values smaller than 1% are difficult to realize because of the reduction of the output level of the oscillator.

C. Summary of the Measurement

Table III gives a summary of the performances of the measured chip.

VIII. CONCLUSION

This circuit shows a one order-of-magnitude improvement in size and in power consumption compared to other architectures. This improvement is due to a reduction of the complexity of the receiver. The RF performance of this circuit is sufficient for a low-range data link. The structure of the receiver allows it to work close to the f_t of the technology (in this case at $f_t/4$). It is possible to improve super-regenerative receivers by further optimization of the operating point and of the quench signal waveform. Operation in regenerative mode seems very promising due to the possibility of reaching much higher selectivity. Low voltage operation, as small as 2 V in this case, is easy to achieve due to the very simple structures of the RF building blocks. Selectivity and sensitivity can be improved by using this receiver in a regenerative mode. This mode of operation seems really promising, due to its absence of limitations in term of selectivity. However, the selectivity of super-regenerative receivers make it incompatible with group special mobile (GSM) or Digital European Cordless Telephone (DECT) operations. Further optimization of this kind of circuit could lead radio transmission to become competitive with infrared transmissions.

REFERENCES

[1] E. H. Armstrong, "Some recent developments of regenerative circuits," *Proc. IRE*, vol. 10, pp. 244–260, Aug. 1922.
[2] H. A. Glucksman, "Superregeneration—An analysis of the linear mode," *Proc. IRE*, vol. 37, pp. 500–504, May 1949.
[3] G. G. Macfarlane and J. R. Whitehead, "The super-regenerative receiver in the linear mode," *Proc. Inst. Elect. Eng.*, vol. 93, pt. III-A, pp. 284–286, Mar./May 1946.
[4] J. R. Whitehead, *Super-Regenerative Receivers*. Cambridge, U.K.: Cambridge Univ. Press, 1950.
[5] A. Vouilloz, M. Declerq, and C. Dehollain, "Selectivity and sensitivity performances of superregenerative receivers," in *Proc. ISCAS'98*.
[6] P. Deval, V. Valence, and F. Anghinolfi, "Low-voltage/low power (100 mW), 2 MHz CMOS comparator for 12-bit ADCS," in *Proc. ISCAS'94*.
[7] F. Krummennacher and N. Joehl, "A 4 MHz CMOS continuous-time filter with on-chip automatic tuning," *IEEE J. Solid-State Circuits*, vol. SC-23, pp. 750–758, June 1988.

Patrick Favre (M'96) was born in Geneva, Switzerland, on May 30, 1965. He received the M.S. degree in electrical engineering from Swiss Federal Institute of Technology (EPFL), Lausanne, in 1992. He is presently pursuing the Ph.D. degree at EPFL.

From 1991 to 1992, he was a Research Assistant at the Electronics Laboratories (LEG) of EPFL, where he designed high-frequencies circuits. In 1992, he joined the wireless group of LOGITECH S.A., where he designed wireless peripherals for personal computers. His Ph.D. dissertation is on the theory and implementation of new architectures of super-regenerative receivers. He hold several patents in the domain of radio communications.

Norbert Joehl was born in Geneva, Switzerland, on May 5, 1959. He received the M.S. and Ph.D. degrees in electrical engineering from Swiss Federal Institute of Technology (EPFL), Lausanne, in 1985 and 1992, respectively.

Since 1985, he has been with the Electronics Laboratory of EPFL, working in the field of low-power and high-performance analog CMOS and BiCMOS integrated circuit design. He is currently Lecturer of Electronic Systems at the Ecole d'Ingnieurs de l'Etat de Vaud and is responsible for research activities at the Electronics Laboratory of EPFL. He is author or co-author of ten scientific publications.

Alexandre Vouilloz was born in Chne-Bougeries, Switzerland, on October 28, 1970. He received the M.Sc. degree in electrical engineering from Swiss Federal Institute of Technology (EPFL), Lausanne, in 1997. Since 1997, he has been working toward the Ph.D. degree at the Electronics Research Laboratory of EPFL.

His Ph.D. dissertation is on the theory of super-regenerative receivers and their CMOS integration for low-power, short-distance applications.

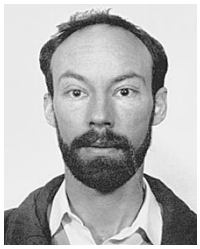

Philippe Deval was born in La Rochelle, France, on July 15, 1960. He received the M.S. and Ph.D. degrees from Swiss Federal Institute of Technology (EPFL), Lausanne, in 1983 and 1992, respectively.

His doctoral research was on high-accuracy A/D converters using dynamic current memories. In 1993 he joined MEAD Microelectronics, where he is Analog Design Manager. His current interests are in low-voltage/low-power mixed digital analog IC design, biomedical ASIC's including low-voltage supplies (1.1 V) and high-voltage output capabilities (15 V to 40 V). He is author and co-author of more than 20 scientific publications.

Catherine Dehollain (M'93) was born on November 20, 1957, in Paris, France. She received the degree of electrical engineer in 1982 and the Ph.D. degree in 1995, both from Swiss Federal Institute of Technology (EPFL), Lausanne.

From 1982 to 1984, she was a Research Assistant at the Electronics Laboratories (LEG) of EPFL, where she designed switched-capacitor filters and studied MOS transistor modelling. In 1984, she joined the Motorola European Center for Research and Development, Geneva, where she designed integrated circuits applied to telecommunications. While with Motorola, she also participated in joint projects with British Telecom and the French Company Alcatel. In 1990, she returned to EPFL as a Senior Assistant at the Chaire des Circuits et Systmes (CIRC) where she worked on impedance broadband matching in the area on electrical filters. Since July 1995, she has been working at LEG EPFL as a Technical Project Manager on wireless data transmission techniques at short distances, operating in UHF frequencies. She is the Project Manager of the Esprit project SUPREGE on the super-regeneration (Project ESD 25400). Since 1998, she has been a Lecturer at EPFL in the area of HF and UHF circuits and techniques. Her technical interests include low-power analog circuit techniques, electrical filters, and impedance broadband matching. She is the author of the book *Adaptation d'impédance à Large Bande* (Lausanne: Presses Polytechniques et Universitaires Romandes, 1996) and a co-author of the book *Filtres Electriques* (Lausanne: Presses Polytechniques et Universitaires Romandes, 1996). She is author or co-author of more than 15 scientific publications.

Michel J. Declercq (S'70–M'72–SM'93) received the Ph.D. degree from the Catholic University of Louvain, Belgium, in 1971.

In 1973, he was awarded a Senior Fulbright Fellowship and joined Stanford University as a Research Associate in the Microelectronics Labs. From 1974 to 1978, he was Research Associate and Lecturer at the Catholic University of Louvain. In 1978, he joined Tractebel (Socit Gnrale de Belgique), in Brussels, Belgium, where he was Group Leader of the Electronic Systems team. In 1985, he joined Swiss Federal Institute of Technology (EPFL), Lausanne, Switzerland, where he is currently Professor and Director of the Electronics Laboratory. His research activities are related to mixed analog-digital I.C. design and design methodologies. He is the author or co-author of more than 130 scientific publications and holds several patents.